Geometric control analysis of the unsteady aerodynamics of a pitching-plunging airfoil in dynamic stall

L. Pla Olea[1] and H. E. Taha[1]
Department of Mechanical and Aerospace Engineering, University of California, Irvine, California 92697, USA.

(*Electronic mail: lplaolea@uci.edu)

(Dated: 26 January 2024)

Geometric control theory is the application of differential geometry to the study of nonlinear dynamical systems. This control theory permits an analytical study of nonlinear interactions between control inputs, such as symmetry breaking or force and motion generation in unactuated directions. This paper studies the unsteady aerodynamics of a harmonically pitching-plunging airfoil in a geometric control framework. The problem is formulated using the Beddoes-Leishman model, a semi-empirical state space model that characterizes the unsteady lift and drag forces of a two-dimensional airfoil. In combination with the averaging theorem, the application of a geometric control formulation to the problem enables an analytical study of the nonlinear dynamics behind the unsteady aerodynamic forces. Results show lift enhancement when oscillating near stall and thrust generation in the post-stall flight regime, with the magnitude of these force generation mechanisms depending on the parameters of motion. These findings demonstrate the potential of geometric control theory as a heuristic tool for the identification and discovery of unconventional phenomena in unsteady flows.

I. INTRODUCTION

Recent developments in Micro-Air Vehicles (MAVs) have spawned an interest in bio-inspired flapping wings. The astonishing maneuverability and flight performance of insects and small birds inspire new designs of more efficient and robust MAVs, but this adaptation of flapping flight to man-made vehicles requires a good understanding of the dynamics of unsteady flows, among many other challenges. In particular, it is important to comprehend the mechanisms behind the generation of the aerodynamic forces in these unsteady regimes and to predict the conditions in which these force generation phenomena occur.

The study of unsteady aerodynamics traces back to the 1920s when Wagner[1] formulated the time response of the lift force experienced by an airfoil due to a step change in its angle of attack. A decade later, Theodorsen[2] provided an analytical solution for the steady state lift response of a harmonically pitching and plunging airfoil. Most of the studies that followed, such as those of von Kármán and Sears[3], Schwarz[4], and Küssner[5], expanded on Theodorsen's work, focusing on the frequency response of the lift force in oscillating airfoils. Similarly, in the 1930s, Garrick[6,7] proposed a model based on Theodorsen's approach to calculate the thrust generated by a flapping airfoil. These reputed classical theories, though restricted to small angles of attack, provide an insight into the several effects that contribute to the unsteady aerodynamic forces, such as the bound circulation, the wake vortices, and the added mass. However, they rely on a small disturbance linear framework that does not permit the discovery of unconventional unsteady mechanisms.

Experimental observations have been pivotal in finding rich unsteady dynamical behavior. Early studies in dynamic stall reported an increase in the lift force past its steady value when performing a dynamic maneuver near stall[8–11]. More recently, computational and experimental efforts focused on the flow characteristics and structures leading to this lift enhancement, such as the contributions of the leading-edge vortex (LEV) and the wake vorticity[12–17]. Similarly, experimental work on oscillatory airfoils uncovered symmetry breaking mechanisms. When oscillating an airfoil, the resulting lift and drag forces are oscillatory, and their mean values may be expected to match their steady counterparts. Nonetheless, there are plenty of examples in the literature[6,12–14,18–21] displaying an increase or decrease in the mean lift and thrust when oscillating at a high enough frequency, revealing a force generation mechanism due to an underlying symmetry breaking. A notable effort in this regard is that of Vandenberghe *et al.*[22], who studied a plunging airfoil in a still fluid. They observed that, past a certain frequency, the airfoil moved spontaneously forward, indicating the generation of a net thrust force.

Thus, most, if not all, of the known force generation mechanisms occurring in unsteady flows have been discovered through smart experimental observations or computational simulations. However, there are, to the authors' knowledge, no theoretical efforts that provide a framework for the systematic discovery of these phenomena. This scarcity of analytical work may be attributed to a lack of appropriate analysis tools. Unconventional unsteady aerodynamics mechanisms usually rely on higher-order flow interactions, and a theoretical study of these interactions requires mathematical tools that do not neglect nonlinearities of the flow dynamics. We believe that geometric control theory[23–27] can bridge this gap and provide a proper framework for the analysis and prediction of known and yet-to-be-discovered unsteady phenomena.

Geometric control theory, a combination of differential geometry and control theory, was first developed in the 1970s by Brockett[23,24] and Sussmann[25–27] with the purpose of studying dynamical systems evolving on *manifolds* or curvy spaces. Instead of neglecting nonlinearities, geometric control theory thrives on them: it analyzes the nonlinear interactions occurring within a system that may lead to the generation of forces in unactuated directions. As such, geometric control theory

has been adopted in the analysis of nonlinear control systems. Its applicability ranges from nonlinear control and motion planning in robotics[28,29], to spacecraft attitude dynamics and control[30–32], to, more recently, bio-inspired flight[33–37].

The nonlinear framework of geometric control theory provides a heuristic formulation for the systematic discovery of non-intuitive unsteady aerodynamics mechanisms. Our first trials in this direction (i.e., applying geometric control tools to unsteady aerodynamics) were encouraging[38,39]. We utilized a previously developed reduced-order model (ROM)[40] to analyze the low-Reynolds aerodynamic loads over a pitching-plunging airfoil in a geometric control framework, which led to the discovery of unconventional lift enhancement and drag reduction mechanisms induced by the pitching and plunging motions.

Similarly, this work is along the same line of research: studying the nonlinear behavior of the average lift and drag forces over a harmonically oscillating airfoil using a geometric control framework. However, in contrast to our previous effort[39], we focus here more on the contributions of the LEV during a harmonic dynamic stall maneuver. To achieve this goal, we need an analytical ROM that accounts for (i) unsteadiness and (ii) nonlinearity, in an (iii) efficient and compact way, with particular emphasis on LEV contributions to dynamic stall. As such, we found the Beddoes-Leishman model[41–43] to be a good candidate for such the sought ROM, for it reasonably captures the unsteady nonlinear aerodynamics of dynamic stall and is represented in a state-space form, which is convenient for dynamical systems analysis, in general, and geometric control and averaging, in particular.

In the present study, we apply the Beddoes-Leishman model to a two-dimensional pitching and plunging airfoil and put it in a form amenable to geometric control theory. The model is then analyzed with a combination of mathematical tools from the averaging theorem and geometric control theories to derive analytical expressions for the mean lift and drag forces. Finally, these expressions are studied to uncover and identify the causes behind lift and thrust enhancement mechanisms. Thus, the main objective of this work is not to calculate the values of the average lift and drag forces but to study their qualitative behavior, which can then be further scrutinized through experimental observations or computational simulations.

The following list summarizes the contributions of the current paper:

- Formulation of the Beddoes-Leishman model in a geometric control framework.
- Geometric control analysis of dynamic stall.
- Analytical study of the averaged lift and drag forces in dynamic stall.
- Presentation of a systematic approach to identify force generation mechanisms due to symmetry breaking in dynamic stall.
- Identification of the key parameters controlling these mechanisms.
- Analysis of the fluid physics behind these mechanisms.

The article is structured as follows. Section II introduces the necessary background on geometric control theory in the analysis of nonlinear dynamical systems, and Section III reviews the Beddoes-Leishman model of dynamic stall. Next, Section IV formulates the problem of the pitching and plunging airfoil in a geometric control framework. Finally, the results are presented in Section V, which applies the proposed geometric control and averaging analysis to the Beddoes-Leishman model. A discussion of the results is provided in the same section.

II. GEOMETRIC CONTROL THEORY

Geometric control theory implements tools from differential geometry for the study of control systems. Developed in the 1970s to analyze nonlinear systems, geometric control theory is concerned with dynamical systems evolving on curvy spaces called manifolds. It was the need for an appropriate mathematical tool to perform calculations on curved domains that invoked a differential geometric formulation of control theory[44], effectively conceiving a geometric control theory. Note that differential-geometric formulation of mechanics preceded the application to control theory by centuries; it can be traced back to Jacobi (1842) and Darboux (1889), see Dugas[45]. This section introduces some of the geometric control concepts to be utilized in the study of unsteady fluid dynamics.

A. Unconventional Force Generation

Consider the finite-dimensional, nonlinear, control-affine system

$$\dot{\boldsymbol{x}}(t) = \boldsymbol{f}(\boldsymbol{x}(t)) + \sum_{j=1}^{m} \boldsymbol{g}_j(\boldsymbol{x}(t))\, u_j(t), \quad \boldsymbol{x} \in \mathbb{M}^n, \qquad (1)$$

where $\boldsymbol{x}$ is a state vector evolving on an $n-$dimensional manifold $\mathbb{M}^n$, $\boldsymbol{f}$ is the drift vector field representing the uncontrolled dynamics of the system, and $\boldsymbol{g}_j$'s are the control vector fields corresponding to the inputs u_j's. In a driftless system ($\boldsymbol{f} = \boldsymbol{0}$), one can move along the vector $\boldsymbol{g}_k$ through direct actuation by turning off all control inputs except for u_k. Geometric control theory allows for expanding the admissible directions of motion by introducing the concept of anholonomy or geometric phases, in which a specific manipulation of the available control inputs may generate forces and, consequently, motion in a direction with no direct actuation[24,46]. These new and additional directions of motion are determined through *Lie bracket* operations between the control vectors (admissible directions of motion) of the system. The Lie bracket between the control vectors $\boldsymbol{g}_j$ and $\boldsymbol{g}_k$ is defined as

$$[\boldsymbol{g}_j, \boldsymbol{g}_k] = \frac{\partial \boldsymbol{g}_k}{\partial \boldsymbol{x}} \boldsymbol{g}_j - \frac{\partial \boldsymbol{g}_j}{\partial \boldsymbol{x}} \boldsymbol{g}_k. \qquad (2)$$

If the Lie product $[\boldsymbol{g}_j, \boldsymbol{g}_k]$ is linearly independent of the two vector fields $\boldsymbol{g}_j$ and $\boldsymbol{g}_k$ that generated it, the resulting Lie bracket indicates a new direction of motion. That is, a specific manipulation of the control inputs u_j and u_k may lead to net motion in an unactuated direction with no direct control authority. The motion along $[\boldsymbol{g}_j, \boldsymbol{g}_k]$ is accomplished with 90° phased square waves or sinusoidal control of the inputs u_j and u_k[28].

B. Higher-Order Averaging of High-Amplitude High-Frequency Periodically Forced Systems

Geometric control theory is interestingly combined with averaging theory[46,47] through the exploitation of chronological calculus[48] for the analysis of time-periodic systems. The combination of these mathematical tools captures higher-order effects occurring in nonlinear systems that are usually neglected by direct averaging[49].

The formal definition of the *averaging theorem* considers the nonlinear, time-periodic system written in the averaging-canonical form[49]

$$\dot{\boldsymbol{x}} = \varepsilon \boldsymbol{X}(\boldsymbol{x}, t, \varepsilon), \tag{3}$$

where ε is a small parameter such that $0 < \varepsilon << 1$, and the vector field $\boldsymbol{X}$ is T-periodic in t. The averaged system corresponding to Eq. (3) is

$$\dot{\bar{\boldsymbol{x}}} = \varepsilon \bar{\boldsymbol{X}}(\bar{\boldsymbol{x}}), \tag{4}$$

where $\bar{\boldsymbol{X}}(\bar{\boldsymbol{x}}) = \frac{1}{T}\int_0^T \boldsymbol{X}(\boldsymbol{x}, \tau, 0) d\tau$, and the over-bar indicates an averaged quantity.

Now, consider a nonlinear system subject to high-amplitude, high-frequency, periodic forcing in the form

$$\dot{\boldsymbol{x}}(t) = \boldsymbol{f}(\boldsymbol{x}(t)) + \frac{1}{\varepsilon}\boldsymbol{G}\left(\boldsymbol{x}(t), \frac{t}{\varepsilon}\right), \tag{5}$$

where the vector field $\boldsymbol{G}$ is T-periodic in its second argument t. The averaging theorem cannot be directly applied to the system in Eq. (5) because it is not in the averaging-canonical form (3). Furthermore, the vector fields $\boldsymbol{f}$ and $\boldsymbol{G}$ are of different orders in ε. Proper averaging of this system requires a more rigorous technique; the Variation of Constants formula usually provides a remedy for this issue[49–54]. It allows decomposing the system (5), which is not directly amenable to the averaging theorem into two different systems, each of which is amenable to the form (3).

If $\boldsymbol{f}$ and $\boldsymbol{G}$ are continuously differentiable and $\boldsymbol{G}$ is a T-periodic, zero-mean vector field, with the aid of the Variation of Constants formula, the averaged dynamics of the system (5) is written as[29,36,48]

$$\dot{\bar{\boldsymbol{x}}}(t) = \bar{\boldsymbol{F}}(\bar{\boldsymbol{x}}(t)), \tag{6}$$

where $\bar{\boldsymbol{F}}(\bar{\boldsymbol{x}}(t)) = \frac{1}{T}\int_0^T \boldsymbol{F}(\boldsymbol{x}(t), \tau)\, d\tau$, and $\boldsymbol{F}$ is the pullback of $\boldsymbol{f}$ along the flow $\Phi_t^{\boldsymbol{G}}$ of the time-varying vector field $\boldsymbol{G}$. For a time-invariant vector $\boldsymbol{f}$ and a time-varying $\boldsymbol{G}$, the pullback vector field $\boldsymbol{F}(\boldsymbol{x}(t), t)$ is obtained through an iteration of Lie brackets between $\boldsymbol{f}$ and $\boldsymbol{G}$

$$\boldsymbol{F}(\boldsymbol{x}(t), t) = \boldsymbol{f}(\boldsymbol{x}(t)) + \mathscr{G}(\boldsymbol{x}(t), t), \tag{7}$$

where

$$\mathscr{G}(\boldsymbol{x}(t), t) = \sum_{k=1}^{\infty} \int_0^t \cdots \int_0^{s_{k-1}} \left(ad_{\boldsymbol{G}(\boldsymbol{x}(t), s_k)} \ldots ad_{\boldsymbol{G}(\boldsymbol{x}(t), s_1)} \boldsymbol{f}(\boldsymbol{x}(t))\right) ds_k \ldots ds_1, \tag{8}$$

with $ad_{\boldsymbol{G}}\boldsymbol{f} = [\boldsymbol{G}, \boldsymbol{f}]$.

For example, the application of the Variation of Constants formula to the nonlinear system (1), with oscillatory inputs $u_j = \omega U_j \cos(\omega t)$ at high enough frequency ω, leads to the averaged dynamics[33,36,49]

$$\dot{\bar{\boldsymbol{x}}} = \boldsymbol{f}(\bar{\boldsymbol{x}}) - \sum_{j,k=1}^{m} \frac{U_j U_k}{4} [\boldsymbol{g}_j, [\boldsymbol{f}, \boldsymbol{g}_k]](\bar{\boldsymbol{x}}). \tag{9}$$

Thus, high-frequency zero-mean oscillations can modify the averaged dynamics of a system, as shown by the last term in Eq. (9), and induce net motion. This contribution is completely ignored when performing direct averaging and only appears when accounting for the higher-order effects of nonlinear systems.

III. BEDDOES-LEISHMAN MODEL

The application of geometric control theory to the study of unsteady flows requires a special formulation of the aerodynamic problem as a dynamical system[55]; i.e, in the form of Eq. (1). Clearly, brute-force application of Navier-Stokes' equations is inappropriate here, so a reduced-order model (ROM) is needed. This ROM has to be rich enough to capture the main physical attributes of unsteady flows, but it also needs to be compact and efficient to allow geometric control analysis of the flow dynamics. The semi-empirical Beddoes-Leismann model[41–43] for dynamic stall reasonably satisfies these requirements.

Initially developed to perform aeroelastic analysis on rotor aircraft, the Beddoes-Leishman model[41–43] provides the unsteady lift, drag, and pitching moment of a two-dimensional airfoil undergoing a dynamic stall maneuver. The model con-

sists of four sets of first-order ordinary differential equations (ODE's) representing different aspects of unsteady flows: (i) attached flow, (ii) dynamic stall onset, (iii) trailing edge separation, and (iv) leading-edge vortex effects. The dynamics of the system are coupled such that the output of one set is the input of the next one, and so on, allowing for an easy transition in the calculations from attached flow to static stall, and then to dynamic stall. Compressibility effects are also included.

A. Attached Flow

The first aspect of the flow to be characterized is the aerodynamic response when the flow is fully attached to the airfoil. The formulation derives from aerodynamic indicial response functions (e.g., Wagner's[1]), generalized for non-zero, subsonic Mach numbers to include compressibility effects. The resulting system employs four aerodynamic states to characterize the force response[41–43]:

$$\dot{\boldsymbol{x}}_{1-4} = \boldsymbol{A}\boldsymbol{x}_{1-4} + \boldsymbol{B}\begin{Bmatrix}\alpha_T \\ q\end{Bmatrix}, \tag{10}$$

$$C_N^p = \boldsymbol{C}\boldsymbol{x}_{1-4} + \boldsymbol{D}\begin{Bmatrix}\alpha_T \\ q\end{Bmatrix}, \tag{11}$$

where $\boldsymbol{x}_{1-4}$ is the vector containing the four states associated with the attached-flow formulation, C_N^p is the normal force coefficient under attached flow conditions, and $q = \frac{2\dot{\alpha}b}{U}$ is the non-dimensional pitch rate. The matrices $\boldsymbol{A} = \mathrm{diag}\,(a_{11}\ a_{22}\ a_{33}\ a_{44})$, $\boldsymbol{B}$, $\boldsymbol{C}$, and $\boldsymbol{D}$ are dependent on the Mach number M and the characteristics of the airfoil. That is, the attached flow dynamical system (10, 11) has two inputs: the angle of attack α_{eff} and the pitch rate q; and one output: the normal force coefficient C_N^p. To include the effect of the plunging velocity $\dot{h}$ on the angle of attack seen by the airfoil, we adopt the concept of total angle of attack α_T, defined as

$$\alpha_T(t) = \alpha(t) + \arctan\frac{\dot{h}}{U},$$

The first two states of Eq. (10) are associated with the circulatory response of the airfoil and the other two with the non-circulatory response. As such, the normal force coefficient C_N^p includes both contributions. The circulatory component of the normal coefficient under attached flow conditions is defined as

$$C_N^C(t) = C_{N_\alpha}\alpha_E(t), \tag{12}$$

where C_{N_α} is the curve slope of the normal force coefficient in the linear regime, and α_E is the effective angle of attack:

$$\alpha_E(t) = \beta^2\left(\frac{U}{b}\right)(A_1 b_1 x_1 + A_2 b_2 x_2), \tag{13}$$

where A_1, A_2, b_1, and b_2 are constants associated with the airfoil indicial response, and $\beta = \sqrt{1-M^2}$ is the compressibility factor.

The original formulation of Beddoes and Leishman[41–43] includes four more states ($\boldsymbol{x}_{5-8}$) to characterize the dynamics of the pitching moment associated with the attached flow response. Since moment calculation is outside the scope of this study, these states have been excluded. Nevertheless, in the following sections, we opt to maintain the original numbering of the Beddoes-Leishmann model for the remaining states, which, unfortunately, creates a gap in the numbering system of this paper.

B. Stall Onset

A critical aspect of dynamic stall modeling is the proposed criterion for leading-edge separation. In the Beddoes-Leishman model, leading-edge separation onset is associated with the attainment of a critical leading-edge pressure, or equivalently, the critical normal force coefficient C_{N_1}[41]. The literature includes other successful criteria, such as the Leading-Edge Suction Parameter (LESP) criterion, proposed by Ramesh, Gopalarathnam, and their colleagues[56–58]. In contrast to the LESP criterion, the Beddoes-Leihsman model assumes lag between the moment when the attached-flow leading-edge pressure (or normal force) reaches a critical value and the onset of leading-edge separation; a first-order lag is assumed:

$$\dot{x}_9 = -\frac{x_9}{T_P} + \frac{C_N^p(t)}{T_P}, \tag{14}$$

$$C_N'(t) = x_9, \tag{15}$$

where x_9 is an internal aerodynamic state variable that represents the first-order lag, and T_P is the corresponding time constant that is determined empirically. The output coefficient $C_N'(t)$, which is a lagged (filtered) version of the attached-flow normal force coefficient, dictates the dynamic stall criterion: leading-edge separation begins when $C_N'(t)$ exceeds a critical value denoted by C_{N_1}.

C. Trailing Edge Separation

The effect of trailing edge separation on the aerodynamic forces is modeled using Kirchhoff's theory[41,42]:

$$C_N = C_{N_\alpha}\left(\frac{1+\sqrt{f'}}{2}\right)^2\alpha, \tag{16}$$

where $f' \in [0,1]$ represents the location of the steady separation point normalized by the airfoil chord; $f \simeq 1$ implies separation near the trailing edge (i.e., attached flow). Its variation with the angle of attack is modeled through the empirical relations[41]

$$f' = \begin{cases} 1 - 0.3\exp\left(\frac{\alpha-\alpha_1}{S_1}\right) & \text{if } \alpha < \alpha_1 \\ 0.04 + 0.66\exp\left(\frac{\alpha_1-\alpha}{S_2}\right) & \text{if } \alpha > \alpha_1 \end{cases}, \tag{17}$$

where α_1 is the angle at which the steady flow separates at 70% of the chord, and S_1 and S_2 are empiric constants utilized to characterize static stall. Note that the angle of attack in Eq. (17) should be replaced with the total angle of attack defined earlier, which accounts for both pitching and plunging.

Consistent with the philosophy of the model, Beddoes and Leishman assumed a first-order lag in trailing edge separation:

$$\dot{x}_{10} = -\frac{x_{10}}{T_f} + \frac{f'\left(\frac{x_9}{C_{N_\alpha}}\right)}{T_f}, \tag{18}$$

$$f''(t) = x_{10}, \tag{19}$$

where f'' is the effective separation point given by the state x_{10}, and T_f is an empirical time constant. The effective separation point then determines the normal force coefficient under trailing edge separation conditions according to the Kirchhoff theory:

$$C_N^f(t) = C_{N_\alpha}\left(\frac{1+\sqrt{f''}}{2}\right)^2 \alpha_E(t), \tag{20}$$

Similarly, the force in the tangential direction (positive in the left direction), or chord force, also depends on the effective separation point as

$$C_C(t) = \eta C_{N_\alpha} \alpha_E^2 \sqrt{f''}, \tag{21}$$

where η is an empirical parameter that provides room for modeled viscous effects.

D. Dynamic Stall

The dynamic stall phenomenon is characterized by the formation of a vortex near the leading edge of the airfoil[8–10,16,17,59]. The vortex grows in size and strength until it separates from the leading edge and convects downstream. According to the Beddoes-Leisman model, vortex detachment occurs when the absolute value of $C_N'(t)$ exceeds C_{N_1}[41,42]. At this point, the non-dimensional counter τ_v is triggered and marches uniformly by the non-dimensional time Ut/b). Simultaneously, the LEV continues to grow during this phase until the instant $\tau_v = 2T_{vl}$, where $2T_{vl}$ is another empirical time constant that represents the time taken by the LEV to reach the trailing edge. At this moment, the contribution of the LEV to the lift force vanishes.

The vortex contribution to the normal force coefficient is given by the internal aerodynamic state variable x_{11}, or $C_N^v(t)$, and is modeled as follows:

$$\dot{x}_{11} = -\frac{x_{11}}{T_v} + \frac{\dot{C}_v}{T_v}, \tag{22}$$

$$C_N^v(t) = x_{11}, \tag{23}$$

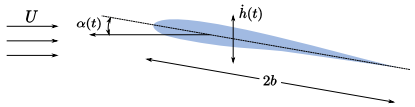

FIG. 1: Schematic diagram of a two-dimensional pitching-plunging airfoil in a free stream.

where

$$C_v = \begin{cases} C_N^C\left[1-\left(\frac{1+\sqrt{f''}}{2}\right)^2\right] & \text{for } \tau_v \le 2T_{vl} \\ 0 \quad \text{for } \tau_v > 2T_{vl} \end{cases}, \tag{24}$$

C_N^C is the attached-flow circulatory normal-force coefficient, and the time constants T_v and T_{vl} are determined empirically.

E. Total Aerodynamic Response

The total normal force coefficient of an airfoil under dynamic stall conditions is the sum of the normal force coefficients due to the LEV C_N^v, the separated-flow contribution C_N^f, and the added-mass (non-circulatory) contribution $C_N^p - C_N^C$:

$$C_N(t) = C_N^f(t) + C_N^v(t) + C_N^p(t) - C_N^C(t), \tag{25}$$

The lift and drag coefficients can then be obtained by projecting the normal and tangential (chordwise) force coefficients in the directions normal and tangential to the flow, respectively:

$$\begin{aligned} C_L(t) &= C_N(t)\cos\alpha(t) + C_C(t)\sin\alpha(t) \\ C_D(t) &= C_N(t)\sin\alpha(t) - C_C(t)\cos\alpha(t) \end{aligned}. \tag{26}$$

IV. PROBLEM DEFINITION

This section poses the fluid mechanics problem under study. Consider a two-dimensional, pitching-plunging airfoil in a free stream flow with velocity U, as shown in Fig. 1. The pitching angle α and the plunging displacement h follow the harmonic motion:

$$\alpha(t) = \alpha^* - A_\alpha\cos(\omega t) \text{ and } h(t) = -Hb\cos(\omega t + \phi), \tag{27}$$

where ω is the frequency of oscillation, α^* is the mean pitching angle, A_α is the amplitude of the pitching motion, H is the amplitude of the plunging displacement normalized by the half-chord b, and ϕ is the phase difference between both motions. The pitching axis is taken at the quarter-chord of the airfoil in this study.

The application of geometric control theory to the study of the Beddoes-Leishman model requires a reformulation of the model as a nonlinear, control-affine system in the following way:

$$\dot{\boldsymbol{x}}(t) = \boldsymbol{f}(\boldsymbol{x}(t)) + \boldsymbol{g}_\alpha(\boldsymbol{x}(t))\ddot{\alpha}(t) + \boldsymbol{g}_h(\boldsymbol{x}(t))\ddot{h}(t), \tag{28}$$

$$\boldsymbol{y}(t) = [C_L(t) \quad C_D(t)]^T, \tag{29}$$

where $\boldsymbol{x}(t)$ is the vector containing the states of the system, $\boldsymbol{y}(t)$ is the output of the system, and $\boldsymbol{f}$ is the drift vector field. The input vector fields $\boldsymbol{g}_\alpha$ and $\boldsymbol{g}_h$ are the control vectors associated with the pitching and plunging inputs. The control inputs of the system are $\ddot{\alpha}$ and $\ddot{h}$, the pitching and plunging accelerations, respectively. The definition of a proper dynamical system requires direct dependence only on the inputs, not on their derivatives. Since the accelerations appear (in the non-circulatory terms), if α and h, or $\dot{\alpha}$ and $\dot{h}$ were chosen as inputs, their derivatives would appear in the dynamical model. Therefore, we chose the accelerations to be the inputs to the dynamic model (28) to ensure a proper dynamical representation:

$$\begin{aligned} u_\alpha &= \ddot{\alpha} = \omega^2 A_\alpha \cos(\omega t) \\ u_h &= \ddot{h} = \omega^2 H b \cos(\omega t + \phi). \end{aligned} \tag{30}$$

This study is concerned with the average unsteady lift and drag forces on an airfoil in a high-velocity free stream subject to high-frequency, small-amplitude oscillations at high angles of attack. Given the different orders of magnitude involved in the problem, it is adequate to define the following scaling:

$$\begin{aligned} A_\alpha = \quad & \mathscr{O}(\varepsilon), \quad H = \mathscr{O}(\varepsilon), \quad \omega = \mathscr{O}\left(\frac{1}{\varepsilon}\right) \\ U = \quad & \mathscr{O}\left(\frac{1}{\varepsilon}\right) \quad \Rightarrow k = \frac{\omega b}{U} = \mathscr{O}(1), \end{aligned} \tag{31}$$

with k being the reduced frequency. ε is a small parameter, such that terms of higher order in ε may be neglected with respect to those of lower order.

V. GEOMETRIC CONTROL AVERAGING ANALYSIS

The Beddoes-Leishman model is reformulated in a geometric control framework, i.e., in the form of Eq. (28). The resulting system of the Beddoes-Leishman model for a pitching-plunging airfoil is thus amenable to geometric control theory:

$$\frac{d}{dt}\begin{pmatrix} x_1 \\ x_2 \\ x_3 \\ x_4 \\ x_9 \\ x_{10} \\ x_{11} \\ \alpha \\ \dot{\alpha} \\ \dot{h} \end{pmatrix} = \begin{pmatrix} -b_1\left(\frac{\beta^2 U}{b}\right)x_1 + \alpha_T + \frac{q}{2} \\ -b_2\left(\frac{\beta^2 U}{b}\right)x_2 + \alpha_T + \frac{q}{2} \\ a_{33}x_3 + \alpha_T \\ a_{44}x_4 + q \\ \frac{U/b}{T_p}\left[C_{N_\alpha}\alpha_E + \frac{1}{M}\left(4a_{33}x_3 + a_{44}x_4\right) - x_9 + \frac{4\alpha_T}{M} + \frac{q}{M}\right] \\ \frac{U/b}{T_f}\left[-x_{10} + f'\left(\frac{x_9}{C_{N_\alpha}}\right)\right] \\ \frac{U/b}{T_v}\left[-x_{11} + \dot{C}_v\right] \\ \dot{\alpha} \\ 0 \\ 0 \end{pmatrix} + \begin{pmatrix} 0 \\ 0 \\ 0 \\ 0 \\ 0 \\ 0 \\ 0 \\ 1 \\ 0 \end{pmatrix}\ddot{\alpha} + \begin{pmatrix} 0 \\ 0 \\ 0 \\ 0 \\ 0 \\ 0 \\ 0 \\ 0 \\ 1 \end{pmatrix}\ddot{h}, \tag{32}$$

with the system (32) being equivalent to

$$\dot{\boldsymbol{x}} = \boldsymbol{f}(\boldsymbol{x}) + \boldsymbol{g}_\alpha(\boldsymbol{x})u_\alpha + \boldsymbol{g}_h(\boldsymbol{x})u_h,$$

where $\boldsymbol{x} = [x_1, x_2, x_3, x_4, x_9, x_{10}, x_{11}, \alpha, \dot{\alpha}, \dot{h}]$ is the state vector, and the control inputs u_α and u_h are the pitching and plunging accelerations $\ddot{\alpha}$ and $\ddot{h}$, respectively. As previously mentioned, the output equation comprises the lift and drag force coefficients:

$$\boldsymbol{y}(t) = [C_L(t) \quad C_D(t)]^T.$$

Plugging in the definitions of the inputs from Eq. (30) and referring to the scaling in Eq. (31), the dynamical system takes the form

$$\begin{aligned} \dot{\boldsymbol{x}} = \quad & \boldsymbol{f}(\boldsymbol{x}) \\ & + \frac{1}{\varepsilon}\left[A_\alpha \omega^2 \boldsymbol{g}_\alpha(\boldsymbol{x})\cos(\omega t) + H b \omega^2 \boldsymbol{g}_h(\boldsymbol{x})\cos(\omega t + \phi)\right]. \end{aligned} \tag{33}$$

As a high-frequency, high-amplitude, time-periodic system, Eq. (34) is not amenable to direct averaging[49]. Besides, since the cosine signal has zero mean, the typical averaging procedure would neglect the effect of the pitching-plunging oscillations. Thus, a more rigorous averaging technique is required, such as the one presented in section II B, which is particularly fitting for this problem.

The application of the Variation of Constants formula to the system in Eq. (32) leads to the average dynamics:

$$\frac{d}{dt}\begin{pmatrix}\bar{x}_1\\ \bar{x}_2\\ \bar{x}_3\\ \bar{x}_4\\ \bar{x}_9\\ \bar{x}_{10}\\ \bar{x}_{11}\\ \overline{\alpha}\\ \dot{\overline{\alpha}}\\ \bar{h}\end{pmatrix} = \begin{pmatrix} -b_1\left(\frac{\beta^2 U}{b}\right)\bar{x}_1+\overline{\alpha}_T+\frac{\overline{q}}{2}\\ -b_2\left(\frac{\beta^2 U}{b}\right)\bar{x}_2+\overline{\alpha}_T+\frac{\overline{q}}{2}\\ a_{33}\bar{x}_3+\overline{\alpha}_T\\ a_{44}\bar{x}_4+\overline{q}\\ \frac{U/b}{T_p}\left[C_{N_\alpha}\overline{\alpha}_E+\frac{1}{M}\left(4a_{33}\bar{x}_3+a_{44}\bar{x}_4\right)-\bar{x}_9+\frac{4\overline{\alpha}_T}{M}+\frac{\overline{q}}{M}\right]\\ \frac{U/b}{T_f}\left[-\bar{x}_{10}+f'\left(\frac{\bar{x}_9}{C_{N_\alpha}}\right)\right]\\ \frac{U/b}{T_v}\left[-\bar{x}_{11}+\dot{C}_v\right]\\ \dot{\overline{\alpha}}\\ 0\\ 0\end{pmatrix} + \begin{pmatrix}\mathscr{G}_1(\overline{\boldsymbol{x}})\\ \mathscr{G}_2(\overline{\boldsymbol{x}})\\ \mathscr{G}_3(\overline{\boldsymbol{x}})\\ 0\\ \mathscr{G}_5(\overline{\boldsymbol{x}})\\ 0\\ \mathscr{G}_7(\overline{\boldsymbol{x}})\\ 0\\ 0\\ 0\end{pmatrix} + \mathscr{O}\left(\varepsilon^3\right) \tag{34}$$

where $\mathscr{G}_i$ denotes the i^{th} component of the vector $\mathscr{G}$, which depends on the states of the system. The indicated entries are the only components of $\mathscr{G}$ that do not vanish after performing the proposed averaging analysis. In addition, as indicated in Eq. (8), the pullback consists of an infinite series of iterated Lie Brackets. In the current analysis, the series is truncated after $\mathscr{O}\left(\varepsilon^2\right)$.

The averaging theorem relates the properties of a nonlinear time-periodic system, such as Eq. (32), to those of its average dynamics. In other words, the stability of some periodic orbit solution of the original nonlinear dynamical system may be inferred from the stability properties of the corresponding equilibrium points of the averaged system in Eq. (34). Its equilibrium is obtained by setting the left-hand side to zero, and solving for the fixed point $\boldsymbol{x}^*$ that satisfies the equation

$$\mathbf{0} = \boldsymbol{f}\left(\boldsymbol{x}^*\right) + \overline{\mathscr{G}}\left(\boldsymbol{x}^*\right),$$

The last two equations of the average dynamics in Eq. (34) imply that the equilibrium of the states $\dot{\alpha}$ and $\dot{h}$ is automatically satisfied, and the $\overline{\alpha}$ equation indicates that $\dot{\alpha}^* = 0$. Taking the averaged plunging speed $\dot{h}^*$ to be zero (otherwise, there will be a net drift upward or downward, which is non-physical) but keeping α^* at an arbitrary value to study the effect of the mean angle of attack on the results, we obtain the following equilibrium values for the internal aerodynamic states:

$$\begin{aligned} x_1^* &= \frac{b}{b_1\beta^2 U}\left(\alpha^* - Hk\sin\phi\right)\\ x_2^* &= \frac{b}{b_2\beta^2 U}\left(\alpha^* - Hk\sin\phi\right)\\ x_3^* &= -a_{33}^{-1}\left(\alpha^* - Hk\sin\phi\right)\\ x_4^* &= 0\\ x_9^* &= C_{N_\alpha}\left(\alpha^* - Hk\sin\phi\right)\\ x_{10}^* &= f'\left(\alpha^* - Hk\sin\phi\right) = x_0^*\\ x_{11}^* &= \dot{C}_v^* \end{aligned} \tag{35}$$

The equilibrium $\boldsymbol{x}^*$ of the average dynamics affects the average value of the lift and drag force coefficients. However, since the force coefficients are not linearly dependent on the states, their average is not simply $C_L(\boldsymbol{x}^*)$ and $C_D(\boldsymbol{x}^*)$. Instead, each state is approximated with the first order expression $x_i(t) = x_i^* + A_{x_i}\cos(\omega t + \phi_i)$, and substituted into a multivariable Taylor series expansion of the lift and drag coefficients around $\boldsymbol{x}^*$:

$$\begin{aligned} y_m &= \sum_{n_1=0}^{\infty}\cdots\sum_{n_d=0}^{\infty}\frac{\left(x_1-x_1^*\right)^{n_1}\ldots\left(x_d-x_d^*\right)^{n_d}}{n_1!\ldots n_d!}\left(\frac{\partial^{n_1+\cdots+n_d}y_m}{\partial x_1^{n_1}\ldots\partial x_d^{n_d}}\right)\left(\boldsymbol{x}^*\right)\\ &= y_m\left(\boldsymbol{x}^*\right) + \sum_{i=1}^{n+5}\frac{\partial y_m\left(\boldsymbol{x}^*\right)}{\partial x_i}\left(x_i-x_i^*\right) + \frac{1}{2!}\sum_{i=1}^{n+5}\sum_{q=1}^{n+5}\frac{\partial^2 y_m\left(\boldsymbol{x}^*\right)}{\partial x_i\partial x_q}\left(x_i-x_i^*\right)\left(x_q-x_q^*\right)+\ldots, \end{aligned} \tag{36}$$

where $y_m(\boldsymbol{x}), m \in (C_L, C_D)$. Finally, the average of the force coefficients over a cycle of motion of the inputs is

$$\bar{y}_m = \frac{1}{T}\int_0^T y_m(t)dt \tag{37}$$

A. Average lift coefficient

The average unsteady lift coefficient over one cycle of motion is found to be

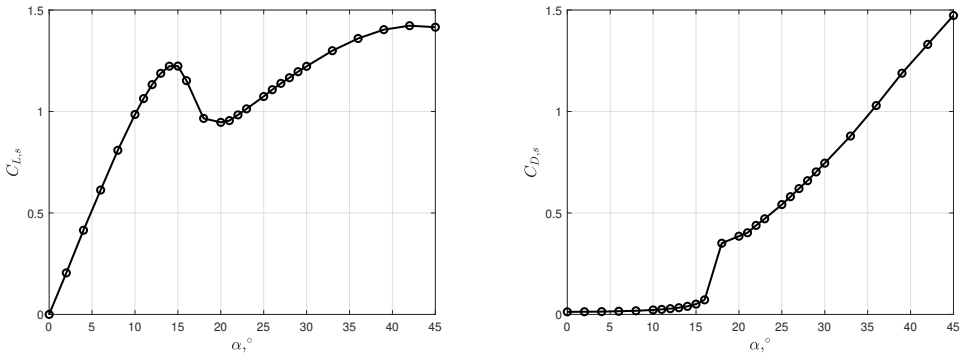

(a) Steady lift coefficient vs. angle of attack.

(b) Steady drag coefficient vs. angle of attack.

FIG. 2: Steady lift and drag coefficients as a function of the angle of attack for a NACA 0012 airfoil at $Re = 5 \cdot 10^5$.

$$\begin{aligned}\overline{C}_L = \quad & \frac{C_{N_\alpha}}{2}\left(\alpha^* - Hk\sin\phi\right)\left[\frac{\left(1+\sqrt{x_0^*}\right)^2}{2}\cos\alpha^* + 2\eta\left(\alpha^* - Hk\sin\phi\right)\sqrt{x_0^*}\sin\alpha^*\right] \\ + \quad & \dot{C}_v^*\cos\alpha^* - \frac{A_\alpha^2}{4}\left\{\frac{C_{N_\alpha}\alpha^*}{2}\left[\frac{\left(1+\sqrt{x_0^*}\right)^2}{2}\cos\alpha^* + 2\eta\alpha^*\sqrt{x_0^*}\sin\alpha^*\right] + \dot{C}_v^*\cos\alpha^* + \frac{8\sin\alpha^*}{M}\right\} \\ + \quad & \frac{2A_\alpha Hk}{M}\sin\alpha^*\sin\phi + \mathscr{O}\left(\varepsilon^3\right), \end{aligned} \tag{38}$$

with the infinite series being truncated at the order $\mathscr{O}\left(\varepsilon^2\right)$. The average lift coefficient is a function of the mean angle of attack α^*, the motion parameters (reduced frequency k and pitching and plunging amplitudes A_α and H, respectively), and the airfoil characteristics. There is also a dependency on the equilibrium values of the average dynamics of the states $x_{10}^* = x_0^*$ and $x_{11}^* = \dot{C}_v^*$, listed in Eq. (35). The equilibrium state x_{10}^* is the point of steady separation evaluated at an equivalent angle of attack $(\alpha^* - Hbk\sin\phi)$, and it can be directly calculated using Eq. (17).

The equilibrium state $x_{11}^* = \dot{C}_v^*$ represents the mean value of the time derivative of Eq. (24), which is obtained by numerical simulation of the Beddoes-Leishman model at different combinations of A_α, H, and k. These data are then used to mathematically represent the relation $\dot{C}_v^* = \dot{C}_v^*\left(\alpha^*, A_\alpha, H, k\right)$ in a smooth way.

The analytical expression of the average lift coefficient in Eq. (38) permits a distillation of the role of each variable in the generation of lift. In fact, one might expect the average lift coefficient $\overline{C}_L$ to be equal to the steady lift coefficient evaluated at the mean angle of attack α^*. However, Eq. (38) uncovers more complex force dynamics due to the oscillatory motion of the airfoil. The first line of the equation is simply the expression of the lift coefficient given by the Beddoes-Leishman model evaluated at the equilibrium points of the averaged dynamics; the first term in brackets is the projection of the normal force coefficient given by Kirchhoff's model in the direction perpendicular to the free stream, and the second term in brackets is the projection of the chord force. Both expressions account for the effect of trailing edge separation. In fact, these two terms in the first line present the average lift coefficient if direct averaging were to be performed on the system without accounting for higher-order effects. Roughly speaking, a deviation of $\overline{C}_L$ from this term may indicate lift enhancement or deficiency and, in essence, the appearance of the symmetry breaking phenomenon. In the following discussion, the two terms in the first line are referred to as the effects of the normal and the tangential forces, respectively.

The second line in Eq. (38) lists two contributions. The first one indicates a clear dependence of the average lift force on the strength of the leading-edge vortex represented by $\dot{C}_v^*$, which is one of the key parameters capturing dynamic stall in the Beddoes-Leishman model. As such, this term implies that the circulation of the leading-edge vortex, which only forms in unsteady conditions, generates a net resulting force even when the airfoil motion is harmonic with zero-mean, and plays a role in breaking symmetry and shifting the average lift force from the steady value. However, given its high dependence on the mean angle of attack and the motion parameters, its contribution to $\overline{C}_L$ can be positive or negative depending on the flight conditions, inducing either lift enhancement or deficiency, respectively.

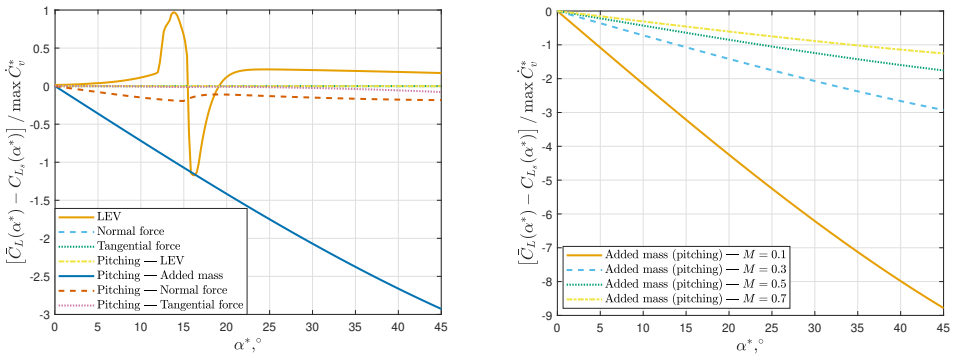

(a) Normalized terms of $\overline{C}_L$ at Mach $M = 0.3$.

(b) Added mass term at different Mach numbers.

FIG. 3: Terms of the average lift coefficient $\overline{C}_L$ minus the same terms for static conditions normalized by the maximum $\dot{C}_v^*$ vs. mean angle of attack α^* for a pitching amplitude of $A_\alpha = 5^\circ$ and a reduced frequency of $k = 0.5$ (NACA 0012 airfoil, $Re = 5 \cdot 10^5$, $H = 0$).

The second contribution groups all the terms that depend explicitly on the pitching motion. The first and second terms are the projections of the normal and the chord forces in the direction perpendicular to the free stream, and they account for the effect of trailing edge separation. Given their positive nature, the role of these terms through the pitching motion is to decrease the average lift coefficient. However, the third term in brackets lists the contribution of the leading-edge vortex due to the pitching motion, and it may take positive or negative values. As such, it may generate a force that increases or decreases $\overline{C}_L$ as a function of the angle of attack and the flight conditions. Lastly, the fourth term in brackets represents the effect of the Mach number on the average lift coefficient, which hints at a decrease in the lift force that is attenuated as the Mach number increases. Due to its non-circulatory nature, this term can also be understood as an expression of the added mass effects.

Finally, the third and last line in Eq. (38) reveals the effect of the interaction between the pitching and plunging motions. The contribution of this combination is unimportant when both movements are in phase. However, the expression suggests a lift enhancement mechanism when the pitching motion lags behind the plunging displacement and lift deficiency when the motion is otherwise. This interactive mechanism diminishes as compressibility effects become more important.

Eq. (38) does not contain any terms that depend solely and directly on the amplitude of the plunging motion, as some terms do on A_α. Nonetheless, the influence of the plunging speed on the average lift coefficient occurs through the leading-edge vortex $\dot{C}_v^*$, whose value is determined by A_α, H, and k. Thus, the effect of the pitching and plunging motions on the average lift coefficient is highly determined by their influence on the rate of change of the leading-edge vortex strength, which is one of the key parameters in the study of dynamic stall behavior.

Before studying the effects of unsteadiness in the lift and drag coefficients, it is necessary to understand their behavior under steady conditions. Fig. 2 shows the steady C_L and C_D as a function of the angle of attack for a NACA 0012 airfoil at $Re = 5 \cdot 10^5$. For this conventional airfoil, the steady lift coefficient increases linearly at low angles of attack until we reach the stall angle (approximately 15°), where lift decreases again until it reaches a minimum point at around 20°. After this trough, lift keeps increasing at a lower rate, reaching another maximum at 42°. On the other hand, at low angles of attack, the drag coefficient increases slowly with α. However, there is a sudden rise in $C_{D,s}$ at stall. At higher angles of attack, the steady drag coefficient keeps increasing significantly.

Fig. 3a shows the value of each of the terms in Eq. (38) when compared to their counterparts under steady conditions for a NACA 0012 airfoil pitching with an amplitude of $A_\alpha = 5^\circ$ at a reduced frequency of $k = 0.5$ and flight Mach number $M = 0.3$ for different mean angles of attack. To do this comparison, the static values have been subtracted from the corresponding terms in Eq. (38) and normalized by the maximum value of $\dot{C}_v^*$ at the amplitude of study, $A_\alpha = 5^\circ$. At $M = 0.3$, the resulting unsteady lift coefficient seems to be dominated by the added mass term (solid blue line), showing the effects of the Mach number, whose magnitude increases with the mean angle of attack. This contribution results in a decrease in $\overline{C}_L$. The second most dominant contribution is due to the leading-edge vortex through $\dot{C}_v^*$ (solid orange line). This term contributes positively to the average lift force when oscillating about mean angles of attack close to the stall angle ($\alpha^* = 15^\circ$). In contrast, in oscillations around a mean angle of attack with a negative steady lift curve slope ($\alpha^* = 15^\circ - 20^\circ$), the leading-edge vortex has a negative impact on the average

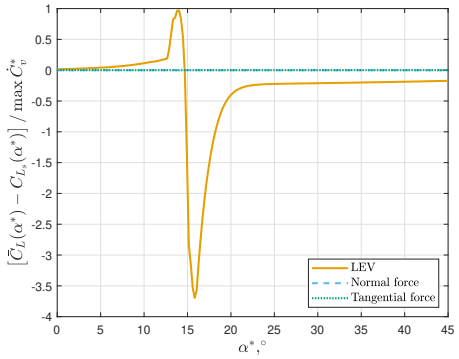

FIG. 4: Terms of the average lift coefficient $\overline{C}_L$ minus the same terms for static conditions normalized by the maximum $\dot{C}_v^*$ vs. mean angle of attack α^* for a plunging motion of effective amplitude $A_{\alpha,eff} = \arctan Hk = 5^\circ$, reduced frequency of $k = 0.5$, and flight Mach number $M = 0.3$ (NACA 0012 airfoil, $Re = 5 \cdot 10^5$, $A_\alpha = 0^\circ$).

$\overline{C}_L$. Interestingly, the terms showing a direct dependence on the pitching amplitude are negligible. This behavior is to be expected because these terms are proportional to the square of the pitching amplitude, and we focus here on small-amplitude oscillations.

The added mass term presented in Eq. (38) is inversely proportional to the Mach number. However, the other contributions in the equation do not present a dependence with M. Fig. 3b depicts the value of the added mass term in Eq. (38) for a NACA 0012 airfoil pitching with an amplitude of $A_\alpha = 5^\circ$ at a reduced frequency of $k = 0.5$ for different mean angles of attack and Mach numbers. The effect of this term is a reduction in the average lift force, although its value is highly dependent on M. At low Mach numbers, the added mass effects are substantial, making them the prevalent unsteady mechanism and leading to an overall decrease in $\overline{C}_L$ at all the studied angles of attack. However, the negative contribution of the added mass term diminishes as the Mach number increases. In fact, at high free stream Mach numbers ($M = 0.5, 0.7$), the positive effect of $\dot{C}_v^*$, occurring when oscillating close to the stall angle, counteracts the negative contribution of M, suggesting lift enhancement in this regime. Since the added mass contribution decreases with M, the other terms in Eq. (38) showing a direct dependence on the pitching amplitude acquire more importance at higher Mach numbers, especially the component of the normal force (dashed red line), which results in a decrease in lift with a maximum value when oscillating at mean angles of attack slightly higher than the stall angle.

Fig. 4 shows the value of each of the terms in Eq. (38) when compared to their steady counterparts for a NACA 0012 airfoil plunging at a reduced frequency of $k = 0.5$ and flight Mach number $M = 0.3$ for different mean angles of attack. The amplitude of the plunging motion is determined by the effective amplitude $A_{\alpha_{\text{eff}}} = \arctan Hk = 5^\circ$, such that the results are comparable to those of the pitching motion. In this case, the leading-edge vortex takes a major role in the enhancement or reduction of the lift force. Similarly to the pitching case, the $\dot{C}_v^*$ term (solid orange line) suggests a positive contribution to the average lift force at mean angles of attack close to the stall angle but a decrease in $\overline{C}_L$ when plunging at post-stall angles of attack where the steady lift curve slope is negative. In the pitching motion, however, the positive and negative contributions of the leading-edge vortex to the lift force were of similar magnitude; in the plunging motion, the negative effect at post-stall is more pronounced than the positive one at stall. The other terms of Eq. (38) are negligible in the studied cases. Interestingly, no considerable dependence on the Mach number is observed in the case of plunging, in contrast to pitching.

B. Average drag coefficient

The average unsteady drag coefficient over one cycle of motion is derived to be

$$\overline{C}_D(\alpha^*) = \frac{C_{N_\alpha}}{2}(\alpha^* - Hk\sin\phi)\left[\frac{\left(1+\sqrt{x_0^*}\right)^2}{2}\sin\alpha^* - 2\eta(\alpha^* - Hk\sin\phi)\sqrt{x_0^*}\cos\alpha^*\right]$$
$$+\dot{C}_v^*\sin\alpha^* - \frac{A_\alpha^2}{4}\left\{\frac{C_{N_\alpha}\alpha^*}{2}\left[\frac{\left(1+\sqrt{x_0^*}\right)^2}{2}\sin\alpha^* - 2\eta\alpha^*\sqrt{x_0^*}\cos\alpha^*\right] + \dot{C}_v^*\sin\alpha^* - \frac{8\cos\alpha^*}{M}\right\}$$
$$-\frac{2A_\alpha Hk}{M}\cos\alpha^*\sin\phi + \mathcal{O}\left(\varepsilon^3\right), \tag{39}$$

with the infinite series being truncated at the order $\mathcal{O}\left(\varepsilon^2\right)$.

The average unsteady drag coefficient $\overline{C}_D$ depends on the mean angle of attack α^*, the motion parameters (A_α, H, and k), the airfoil characteristics such as the slope of the normal force curve C_{N_α} and the separation point x_0^*, and the equilibrium value of the derivative of the vortex strength $\dot{C}_v^*$. Similar to the average lift coefficient, the first line in Eq. (39) is simply the expression of the drag coefficient as given by the Beddoes-Leishman model in Eq. (26) evaluated at the equilibrium points of the averaged dynamics. For instance, the first

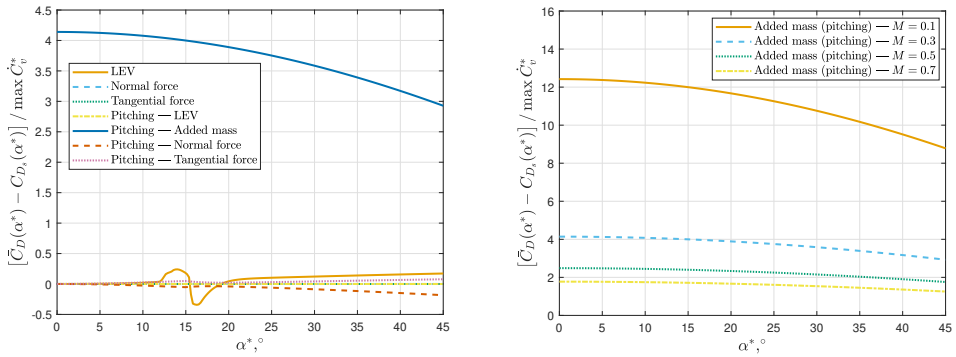

(a) Normalized terms of $\overline{C}_D$ at Mach $M = 0.3$.

(b) Added mass term at different Mach numbers.

FIG. 5: Terms of the average drag coefficient $\overline{C}_D$ minus the same terms for static conditions normalized by the maximum $\dot{C}_v^*$ vs. mean angle of attack α^* for a pitching amplitude of $A_\alpha = 5^\circ$ and a reduced frequency of $k = 0.5$ (NACA 0012 airfoil, $Re = 5 \cdot 10^5$, $H = 0$).

and second terms represent the components of the normal and tangential force coefficients, respectively, in the direction of the free stream. Therefore, as it occurred with the lift coefficient, roughly speaking, a deviation of $\overline{C}_D$ from this expression may entail drag reduction or augmentation as a result of unsteady motion.

The first term in the second line of Eq. (39) shows the effect of the leading-edge vortex on the average drag coefficient. However, since $\dot{C}_v^*$ is highly dependent on the mean angle of attack and the motion parameters, its net effect on the average drag force is intricate and needs some scrutiny, as demonstrated in the discussions of Fig. 5, 6 below. The next term in the second line (the bracketed terms) collects all the terms that depend directly on the amplitude of the pitching motion A_α. The last term in brackets notes the dependence of $\overline{C}_D$ on the Mach number through added mass effects, which decreases as compressibility effects become more important. Interestingly, some of the terms in brackets contribute to a reduction in the drag force, hinting at a possible thrust generation mechanism.

Lastly, the final line of Eq. (39) shows the impact of the combination of both pitching and plunging motions, which also vanishes if both oscillations are in phase. Of particular interest is the case when the plunging motion lags behind the pitching oscillations; in this case, the interactive term becomes negative, pointing to a possible drag reduction mechanism. However, the effect of this interactive mechanism decreases as the Mach number increases.

As it occurred with $\overline{C}_L$, the average drag coefficient does not contain any terms that depend solely and explicitly on the plunging amplitude. However, the dependence of $\overline{C}_D$ on the plunging motion takes place through the average value of the leading-edge vortex strength $\dot{C}_v^*$, which heavily depends on the motion parameters A_α, H and k. Fig. 5a shows the value of each of the terms in Eq. (39) in comparison to their steady counterparts for a NACA 0012 airfoil pitching with an amplitude of $A_\alpha = 5^\circ$ at a reduced frequency of $k = 0.5$ and flight Mach number $M = 0.3$ for different mean angles of attack. Fig. 5b shows the added mass contribution of Eq. (39), the only term to show dependence with M, at different Mach numbers. As it occurred with the lift coefficient, the added mass term (solid blue line in Fig. 5a) dominates over the others. However, contrary to $\overline{C}_L$, even though this contribution decreases with M, as seen in Fig. (5b), its effect is prevalent even at the highest Mach numbers. This relevance implies an increase of the drag force in all flight conditions, although this increment is lower when pitching at higher angles of attack. Nonetheless, Fig. 5a also shows a decrease in the drag force due to a negative contribution of the leading-edge vortex decreasing the drag force when oscillating at angles of attack in the post-stall regime. Similarly, the normal force contributes negatively to $\overline{C}_D$ as the airfoil pitches at higher α^*. However, such effects are negligible when compared to the added mass term.

Fig. 6 shows the value of each of the terms in Eq. (39) when compared to the same terms under steady conditions for a NACA 0012 airfoil plunging at a reduced frequency of $k = 0.5$ and flight Mach number $M = 0.3$ with an effective amplitude of $A_{\alpha_{\text{eff}}} = \arctan Hk = 5^\circ$ for different mean angles of attack. Similar to the lift coefficient, in the case of the plunging motion, the leading-edge vortex seems to be the dominant factor in controlling the average drag coefficient. In fact, the depicted trends are similar to the lift case, which indicates that lift and drag are just two components of the resultant aerodynamic force. Drag increases right before stall and decreases between the stall angle and the trough of the steady lift curve, with the drag reduction being more pronounced than the increase. As shown for $\overline{C}_L$, this increase and decline in the drag coefficient is not considerably dependent on the Mach num-

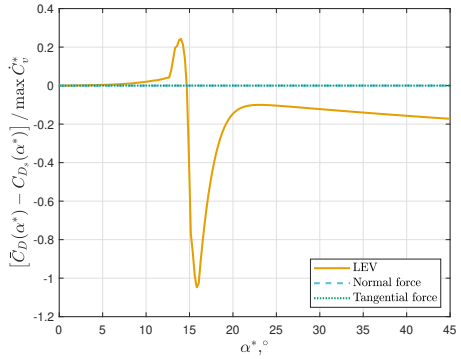

FIG. 6: Terms of the average drag coefficient $\overline{C}_D$ minus the same terms for static conditions normalized by the maximum $\dot{C}_v^*$ vs. mean angle of attack α^* for a plunging motion with an effective amplitude $A_{\alpha,eff} = \arctan Hk = 5°$, reduced frequency of $k = 0.5$, and flight Mach number $M = 0.3$ (NACA 0012 airfoil, $Re = 5 \cdot 10^5$, $A_\alpha = 0°$).

ber. The rest of the terms in Eq. (39) are also negligible, as they were for the lift coefficient.

VI. CONCLUSIONS

Proper analysis of unsteady fluid dynamics systems requires special mathematical tools that account for the higher-order effects due to nonlinear interactions between different flow mechanisms. This paper demonstrates the potential of geometric control theory as an analytical instrument for the study of unsteady fluid dynamics problems.

This work starts by introducing the capacity of geometric control theory to predict phenomena stemming from nonlinear effects, such as the generation of forces or motion in unactuated directions, or the capture of symmetry breaking due to high-frequency oscillatory controls. However, the application of geometric control theory to fluid dynamics requires the formulation of a reduced-order model that is able to capture the major physical aspects of unsteady flows. At the same time, the model needs to be compact to permit a subsequent analytical study of the results. The current paper focuses on the Beddoes-Leishman model for dynamic stall, which comprises both characteristics. The model is applied to a two-dimensional pitching and plunging airfoil performing low-amplitude, high-frequency oscillations. With a combination of geometric control theory and averaging, the current formulation provides the average unsteady lift and drag forces on the oscillating airfoil. The results are thus compared to the steady values to assess any possible enhancement or attenuation in the aerodynamic forces due to the unsteady motion.

The application of geometric control theory to a high-frequency, low-amplitude pitching-plunging airfoil reveals symmetry breaking in both lift and drag forces. Moreover, the rate of change in the strength of the leading-edge vortex is the main parameter governing these force generation mechanisms. The positive contribution of the vortex when oscillating around stall leads to lift enhancement, or an increase in the average lift force, when compared to its steady value. When the oscillation occurs in the post-stall region, the negative rate of change in the vortex strength reduces the average lift on the airfoil. Both pitching and plunging motions depict the aforementioned results, with the enhancement/reduction being controlled by the reduced frequency and the amplitude of motion. However, compressibility also plays a major role in pitching airfoils in this lift enhancement process. That is, pitching oscillations need to occur at high Mach numbers to induce substantial lift enhancement.

Although leading-edge vortex effects are observed in the unsteady drag coefficient of pitching airfoils, their contribution is negligible with respect to the added mass effects. This Mach-dependent contribution, which is dominant over the other effects, suggests an increase in the drag force due to the pitching motion at all mean angles of attack. However, the effect is mitigated at higher angles of attack and high Mach numbers.

On the other hand, the leading-edge vortex dictates the increment and reduction in the drag force of plunging airfoils. The positive rate of change in the vortex strength at stall increases the average drag force of a plunging airfoil when compared to a steady wing. Nonetheless, in the post-stall regime, the leading-edge vortex yields a significant reduction in drag. In fact, the present analysis suggests the generation of a thrust force that overcomes the aerodynamic drag, propelling the airfoil forward. However, this thrust mechanism only occurs when the airfoil is plunging above the stall angle.

The identification of the parameters governing the increase and decrease in the aerodynamic forces of airfoils in unsteady motion provides a better understanding of the higher-order interactions occurring in unsteady flows. These results provide practical knowledge to the relatively unexplored unsteady flight regime, which offers significant potential for revolutionary concepts needed for the next generation of flying vehicles, such as air taxis and drones. Flapping flight, helicopters, and air taxis are inherently time-periodic systems that may readily benefit from the conclusions presented in this work. The cognizance of the mechanisms behind lift enhancement and thrust production may provide substantial insight into these time-periodic systems and, in turn, inspire more efficient, robust, and specialized aircraft. The present paper is one of the first steps in this route, providing efficient analysis tools and a framework that allows the investigation of unconventional flying vehicles employing unsteady aerodynamic phenomena for more efficient performance.

ACKNOWLEDGMENTS

The first author would like to acknowledge the fruitful discussions with N. Khalifa at the University of Califonia, Irvine. This work was supported by the National Science Foundation (NSF) grant number CMMI-1846308.

DATA AVAILABILITY STATEMENT

The data that support the findings of this study are available from the corresponding author upon reasonable request.

[1]H. Wagner, "Über die Entstehung des dynamischen Auftriebes von Tragflügeln," Mathematica **5**, 17–35 (1925).
[2]T. Theodorsen, "General theory of aerodynamic instability and the mechanism of flutter," Tech. Rep. NACA-TR-496 (National Advisory Committe for Aeronautics, Hampton, 1935).
[3]T. von Kármán and W. R. Sears, "Airfoil theory for non-uniform motion," Journal of the Aeronautical Sciences **5**, 379–390 (1938).
[4]L. Schwarz, "Berechnung der druckverteilung siner harmonisch sich verformungen tragfläche in ebener stromung," Luftfahrtforschungr **17**, 379–386 (1940).
[5]H. G. Küssner, "Zusammenfassender Bericht über den instationären Auftrieb von Flügeln," Luftfahrtforschung **13**, 410–424 (1936).
[6]I. E. Garrick, "Propulsion of a flapping and oscillating airfoil," Tech. Rep. NACA-TR-567 (National Advisory Committee for Aeronautics, Hampton, 1936).
[7]H. E. Taha, "Can flapping propulsion boost airplane technology? The flapping-tail concept airplane," AIAA Aerospace Sciences Meeting, 2018 (2018), 10.2514/6.2018-0547.
[8]W. J. McCroskey, "Some current research in unsteady fluid dynamics," Journal of Fluids Engineering **99**, 8–39 (1977).
[9]K. W. McAlister, S. L. Pucci, W. J. McCroskey, and L. W. Carr, "An experimental study of dynamic stall on advanced airfoil sections - Volume 2. Pressure and force data," Tech. Rep. (NASA, Moffett Field, California, 1982).
[10]L. W. Carr, "Progress in analysis and prediction of dynamic stall," Journal of Aircraft **25**, 6–17 (1988).
[11]T. Lee and P. Gerontakos, "Investigation of flow over an oscillating airfoil," Journal of Fluid Mechanics **512**, 313–341 (2004).
[12]D. Rival and C. Tropea, "Characteristics of pitching and plunging airfoils under dynamic-stall conditions," Journal of Aircraft **47**, 80–86 (2010).
[13]D. E. Rival, J. Kriegseis, P. Schaub, A. Widmann, and C. Tropea, "Characteristic length scales for vortex detachment on plunging profiles with varying leading-edge geometry," Experiments in Fluids **55**, 1–8 (2014).
[14]D. J. Cleaver, Z. Wang, I. Gursul, and M. R. Visbal, "Lift enhancement by means of small-amplitude airfoil oscillations at low Reynolds numbers," AIAA Journal **49**, 2018–2033 (2011).
[15]M. R. Visbal, "Control of dynamic stall on a pitching airfoil using high-frequency actuation," 53rd AIAA Aerospace Sciences Meeting (2015), 10.2514/6.2015-1267.
[16]M. R. Visbal and D. J. Garmann, "Dynamic stall of a finite-aspect-ratio wing," AIAA Journal **57**, 962–977 (2019).
[17]P. Ansell, "The onset of dynamic stall: Understanding flowfield unsteadiness to enable closed-loop control," Tech. Rep. (University of Illinois, 2019).
[18]J. Lighthill, "Aerodynamic aspects of animal flight," in *Swimming and Flying in Nature*, edited by T. Y.-T. Wu, C. J. Brokaw, and C. Brennen (Springer, Boston, MA, 1975) 1st ed., pp. 423–491.
[19]K. V. Rozhdestvensky and V. A. Ryzhov, "Aerohydrodynamics of flapping-wing propulsors," Progress in Aerospace Sciences **39**, 585–633 (2003).
[20]I. Gursul and D. Cleaver, "Plunging oscillations of airfoils and wings: Progress, opportunities, and challenges," AIAA Journal **57**, 3648–3665 (2019).
[21]J. M. Anderson, K. Streitlien, D. S. Barrett, and M. S. Triantafyllou, "Oscillating foils of high propulsive efficiency," Journal of Fluid Mechanics **360**, 41–72 (1998).
[22]N. Vandenberghe, J. Zhang, and S. Childress, "Symmetry breaking leads to forward flapping flight," Journal of Fluid Mechanics **506**, 147–155 (2004).
[23]R. W. Brockett, "System theory on group manifolds and coset spaces," SIAM Journal on Control and Optimization **10**, 265–284 (1972).
[24]R. W. Brockett, "Nonlinear systems and differential geometry," Proceedings of the IEEE **64**, 61–72 (1976).
[25]H. J. Sussmann and V. Jurdjevic, "Controllability of nonlinear systems," Journal of Differential Equations **12**, 95–116 (1972).
[26]H. J. Sussmann, "Orbits of families of vector fields and integrability of distributions," Transactions of the American Mathematical Society **180**, 171–188 (1973).
[27]H. J. Sussmann, "A general theorem on local controllability," SIAM Journal on Control and Optimization **25**, 158–194 (1987).
[28]R. M. Murray and S. S. Sastry, "Nonholonomic motion planning. Steering using sinusoids," IEEE Transactions on Automatic Control **38**, 700–716 (1993).
[29]F. Bullo and A. D. Lewis, *Texts in applied mathematics*, edited by J. Marsden, L. Sirovich, and M. Golubitsky, Vol. 49 (Springer, New York, 2004).
[30]P. E. Crouch, "Spacecraft attitude control and stabilization: Applications of geometric control theory to rigid body models," IEEE Transactions on Automatic Control **29**, 321–331 (1984).
[31]G. C. Walsh and S. Sastry, "On reorienting linked rigid bodies using internal motions," in *Proceedings on the 30th Conference on Decision and Control* (Brighton, England, 1991) pp. 1190–1195.
[32]S. S. Sastry, *Nonlinear systems: Analysis, stability, and control*, edited by J. Marsden, L. Sirovich, and S. Wiggins, Interdisciplinary Applied Mathematics, Vol. 10 (Springer-Verlag New York, New York, NY, 1999).
[33]H. E. Taha, C. A. Woolsey, and M. R. Hajj, "Geometric control approach to longitudinal stability of flapping flight," Journal of Guidance, Control, and Dynamics **39**, 214–226 (2016).
[34]S. Tahmasian and C. A. Woolsey, "Flight control of biomimetic air vehicles using vibrational control and averaging," Journal of Nonlinear Science **27**, 1193–1214 (2017).
[35]I. Mir, H. Taha, S. A. Eisa, and A. Maqsood, "A controllability perspective of dynamic soaring," Nonlinear Dynamics **94**, 2347–2362 (2018).
[36]A. M. Hassan and H. E. Taha, "Differential-geometric-control formulation of flapping flight multi-body dynamics," Journal of Nonlinear Science **29**, 1379–1417 (2019).
[37]H. E. Taha, M. Kiani, T. L. Hedrick, and J. S. Greeter, "Vibrational control: A hidden stabilization mechanism in insect flight," Science Robotics **5**, 1–12 (2020).
[38]H. E. Taha, "Geometric nonlinear control of the lift dynamics of a pitching-plunging wing," in *AIAA Scitech 2020 Forum*, January (2020) pp. 1–13.
[39]H. E. Taha, L. Pla Olea, N. Khalifa, C. Gonzalez, and A. S. Rezaei, "Geometric-control formulation and averaging analysis of the unsteady aerodynamics of a wing with oscillatory controls," Journal of Fluid Mechanics **928** (2021), 10.1017/jfm.2021.826.
[40]H. E. Taha, M. R. Hajj, and P. S. Beran, "State-space representation of the unsteady aerodynamics of flapping flight," Aerospace Science and Technology **34**, 1–11 (2014).
[41]J. G. Leishman and T. S. Beddoes, "A semi-empirical model for dynamic stall," Journal of the American Helicopter Society **34**, 3–17 (1989).
[42]J. G. Leishman and G. L. Crouse, "State-space model for unsteady airfoil behavior and dynamic stall," in *30th Structures, Structural Dynamics and Materials Conference* (1989) p. 1319.
[43]J. G. Leishman, *Principles of helicopter aerodynamics*, 2nd ed. (Cambridge University Press, 2006).
[44]R. Brockett, "The early days of geometric nonlinear control," Automatica **50**, 2203–2224 (2014).
[45]R. Dugas, *A history of mechanics* (Dover, 1988).
[46]F. Bullo, "Averaging and vibrational control of mechanical systems," SIAM Journal on Control and Optimization **41**, 542–562 (2003).
[47]P. A. Vela, K. A. Morgansen, and J. W. Burdick, "Underwater locomotion from oscillatory shape deformations," in *Proceedings of the IEEE Conference on Decision and Control*, Vol. 2 (Las Vegas, Nevada USA, 2002) pp. 2074–2080.
[48]A. A. Agrachev and R. V. Gamkrelidze, "The exponential representation of flows and the chronological calculus," Matematicheskii Sbornik **149**, 467–532 (1978).
[49]M. Maggia, S. A. Eisa, and H. E. Taha, "On higher-order averaging of time-periodic systems: reconciliation of two averaging techniques," Nonlinear Dynamics **99**, 813–836 (2020).
[50]J. A. Sanders and F. Verhulst, *Averaging methods in nonlinear dynamical systems* (Springer, New York, 1985).
[51]A. H. Nayfeh, *Perturbation methods* (John Wiley & Sons, 1973).
[52]A. H. Nayfeh and D. T. Mook, *Nonlinear oscillations* (John Wiley & Sons, 1979).

[53] A. H. Nayfeh, *Introduction to perturbation techniques* (John Wiley & Sons, 1981).
[54] A. H. Nayfeh and B. Balachandran, *Applied nonlinear dynamics: analyical, computational, and experimental methods* (John Wiley & Sons, 1995).
[55] H. E. Taha and A. S. Rezaei, "On the high-frequency response of unsteady lift and circulation: A dynamical systems perspective," Journal of Fluids and Structures **93**, 102868 (2020).
[56] K. Ramesh, A. Gopalarathnam, K. Granlund, M. V. Ol, and J. R. Edwards, "Discrete-vortex method with novel shedding criterion for unsteady aerofoil flows with intermittent leading-edge vortex shedding," Journal of Fluid Mechanics **751**, 500–538 (2014).
[57] S. Narsipur, P. Hosangadi, A. Gopalarathnam, and J. R. Edwards, "Variation of leading-edge suction during stall for unsteady aerofoil motions," Journal of Fluid Mechanics (2020), 10.1017/jfm.2020.467.
[58] A. Saini, S. Narsipur, and A. Gopalarathnam, "Leading-edge flow sensing for detection of vortex shedding from airfoils in unsteady flows," Physics of Fluids **33** (2021), 10.1063/5.0060600.
[59] N. M. Khalifa, A. Rezaei, and H. E. Taha, "On computational simulations of dynamic stall and its three-dimensional nature," Physics of Fluids **35** (2023), 10.1063/5.0170251.